Strojniški vestnik - Journal of Mechanical Engineering 68(2022)9, 529-541

DOI:10.5545/sv-jme.2022.15
Original Scientific Paper
Received for review: 2022-01-17
Received revised form: 2022-07-07
Accepted for publication: 2022-08-26

MTPA- and MSM-based Vibration Transfer of 6-DOF Manipulator for Anchor Drilling

Youyu Liu[1,3] – Liteng Ma[1,3] – Siyang Yang[1,3] – Liang Yuan[2] – Bo Chen[1,3]
[1] Key Laboratory of Advanced Perception and Intelligent Control of High-end Equipment, Ministry of Education, China
[2] Technology Department, Wuhu Yongyu Automobile Industry Co., China
[3] School of Mechanical Engineering, Anhui Polytechnic University, China

An anchor drilling for a coal mine support system can liberate an operator from heavy work, but will cause serious vibration, which will be transmitted to the pedestal from the roof bolter along a manipulator. Based on the multi-level transfer path analysis (MTPA) and modal superposition method (MSM), a vibration transfer model for the subsystem composed of the joints of a manipulator with six degrees of freedom (DOF) was established. Moreover, its frequency response function matrix was also built. The 6-DOF excitation of the roof bolter was deduced. The exciting force on the roof bolter transmitted to the pedestal along the 6-DOF manipulator was analysed with a force Jacobian matrix, to identify the external loading on the pedestal. A case in engineering practice shows that the amplitude of each DOF of the pedestal from large to small is as follows: bending vibration (component 1), longitudinal vibration, torsional vibration, bending vibration (component 2), rotational vibration around z-axis, rotational vibration around y-axis. The pedestal is mainly in the form of bending vibration. The theory of vibration transfer along the 6-DOF manipulator for anchor drilling proposed in this article can provide a theoretical foundation for the development of vibration-damping techniques and the design of absorbers.
Keywords: manipulator, multi-level transfer path analysis, modal superposition method, vibration transfer, force Jacobian matrix

Highlights
- *Based on MTPA and MSM, a mathematical model of vibration transfer of a 6-DOF manipulator for anchor drilling is established.*
- *The external loading of the response point of the manipulator pedestal is analysed by using the force Jacobian matrix.*
- *The vibration responses on each DOF of the pedestal and the resonance frequency are obtained.*
- *The case studied in an engineering practice shows that the pedestal is mainly in the form of bending vibration.*

0 INTRODUCTION

Roof bolters are key mechanical equipment for a coal mine supporting system. In the past, drilling was done manually. Working in an area with high concentrations of dust for a long time, workers' physical and mental health will be seriously threatened. At present, the development of a coal mine tunnel support tends to be automatic and intelligent. The manual labour of roof bolters has been gradually replaced by mechanical clamping [1]. An operator can control the roof bolter to drill automatically by human-computer interaction, which can liberate the operator from heavy work, and improve the stability and safety of the coal mine support. Due to the comprehensive excitation of different geotechnical parameters, axial thrust, torque and other factors, there are complex vibrations on drill strings during construction. The main forms include bending vibration, longitudinal vibration, and torsional vibration, which interact with each other to form a nonlinear coupled vibration [2]. The excitation vibration of each degree of freedom (DOF) of the roof bolter is transmitted to the pedestal along a manipulator, which causes the manipulator to vibrate violently, shorten its service life, and then affect the support effect.

Transfer path analysis (TPA) is a tool to study vibration transfer [3] and [4]. There are several methods, such as operational transfer path analysis (OTPA) [5] and [6], global transmissibility direct transmissibility (GTDT) [7] and [8], inverse substructure TPA (ITPA) [9], multi-level transfer path analysis (MTPA) [10] and [11], and so on. Lee and Lee [5] proposed the OTPA method using an emerging deep neural network model, which can successfully predict the path contributions using only operational responses. Yoshida and Tanaka [6] attempted to calculate the vibration mode contribution by modifying OTPA, and then considered the relationship between the principal component and the vibration mode, as well as the associated the principal components with the vibration modes of a test structure. High contributing vibration modes to the response point have been found. It is easily disturbed by factors such as excitation coupling and noise employing this method when calculating the transfer matrix. Wang [7] developed further the prediction capabilities of the GTDT method, which can predict a new response using measured variables of an original system, even though operational

*Corr. Author's Address: Anhui Polytechnic University, Wuhu, China, ahpulyy@163.com

forces are unknown. Guasch [8] addressed some issues concerning the prediction capabilities of the GTDT method when blocking transfer paths in a mechanical system and outlined differences with the more standard force TPA. Wang [9] developed the SDD method further by considering the mass effect of resilient links, which can identify decoupled transfer functions accurately, whilst eliminating the mass effect of resilient links. However, its manoeuvrability is poor for a serial system with many substructures. Gao [11] used MTPA to find the critical paths of seat jitter caused by dynamic unbalance excitation of the drive shaft. The key technology of this method is to identify the external excitation loading, which has good operability for series system.

For the vibration problem of pedestal from manipulator caused by the excitation of a roof bolter, a response amplitude matrix in pedestal is established by the modal superposition method (MSM) in this article. According to the excitation of the roof bolter, the external loading of the response point of the manipulator pedestal is analysed using the force Jacobian matrix. The 6-DOF frequency response function of each subsystem of the manipulator is derived by MTPA, and then the frequency response matrix is constructed, which can solve the problem of Transfer path analysis with low accuracy and poor operability. It will provide a theoretical foundation for the development of vibration damping techniques and the design of absorbers.

1 MULTI-LEVEL TRANSFER PATH ANALYSIS

To reduce the influence of non-important factors while analysing the vibration transfer of manipulator for anchor drilling, some simplifications are made as follows. 1) Each linkage of the manipulator is equivalent to a bar with uniform mass; 2) some transfer mechanisms, such as belt driving and harmonic decelerator in the manipulator, are equivalent to linear massless springs; 3) the modal parameters of the manipulator are linear, namely, the output caused by any combined input are equal to the combination of respective outputs; 4) it satisfies the assumption of time-invariance [12], namely, the dynamic properties of the system are not vary with time. According to the above simplifications, a vibration transfer model of the manipulator for anchor drilling is established, as shown in Fig. 1.

This is a multi-input and multi-output system, in which the six joints of the manipulator are connected in series. The vibration source is the roof bolter that provides excitation; the vibration receiver is the pedestal. The manipulator can be divided into six subsystems by the rotating joint. The external loading of the J_6-subsystem is the excitation from the roof bolter; that of other subsystems is the output of the previous subsystem. The output (response point) of the subsystem is the input (exciting point) of the next subsystem. Nevertheless, the output of the J_1-subsystem acts on the pedestal. According to different excitations of spatial degrees of freedom, each subsystem has *m* inputs and *n* outputs.

According to MTPA, the transfer function of manipulator for anchor drilling can be expressed by the product of the transfer functions of all subsystems [11].

$$\mathbf{H} = \mathbf{H}_{J_1} \mathbf{H}_{J_2} \cdots \mathbf{H}_{J_6}. \tag{1}$$

The vibration response of the excitation from the roof bolter transmitted to the pedestal is expressed as follows.

$$\mathbf{S} = \mathbf{HF}. \tag{2}$$

2 MODAL SUPERPOSITION METHOD

2.1 Response Amplitude Matrix

The dynamic equation of the manipulator for anchor drilling is as follows.

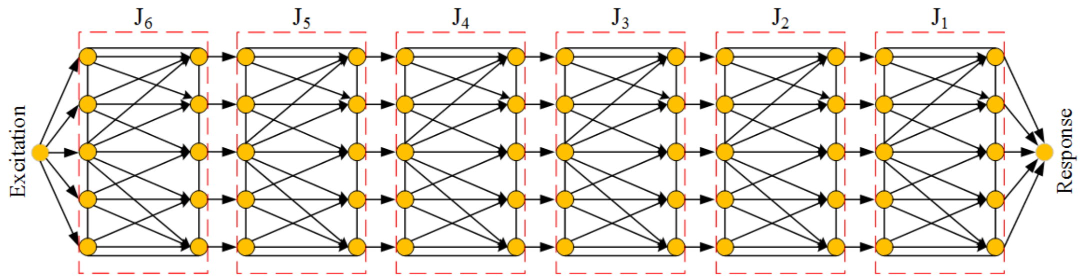

Fig. 1. *Vibration Transfer model of the manipulator*

$$\mathbf{M}\ddot{\mathbf{S}}+\mathbf{C}\dot{\mathbf{S}}+\mathbf{K}\mathbf{S}=\mathbf{F}. \tag{3}$$

According to the linear hypothesis [12], the displacement column vectors of each subsystem of the manipulator can be expressed as the linear addition of each order of modal shapes.

$$\mathbf{S}=\sum_{a=1}^{n} q_a \boldsymbol{\lambda}_a. \tag{4}$$

Substituting Eq. (4) into Eq. (3), then,

$$\mathbf{M}\sum_{a=1}^{n}\ddot{q}_a\boldsymbol{\lambda}_a+\mathbf{C}\sum_{a=1}^{n}\dot{q}_a\boldsymbol{\lambda}_a+\mathbf{K}\sum_{a=1}^{n}q_a\boldsymbol{\lambda}_a=F. \tag{5}$$

Both ends of Eq. (5) are multiplied by $\boldsymbol{\lambda}_b^{\mathrm{T}}$, then,

$$\boldsymbol{\lambda}_b^{\mathrm{T}}\mathbf{M}\left(\sum_{a=1}^{n}\ddot{q}_a\boldsymbol{\lambda}_a\right)+\boldsymbol{\lambda}_b^{\mathrm{T}}\mathbf{C}\left(\sum_{a=1}^{n}\dot{q}_a\boldsymbol{\lambda}_a\right)+\boldsymbol{\lambda}_b^{\mathrm{T}}\mathbf{K}\left(\sum_{a=1}^{n}q_a\boldsymbol{\lambda}_a\right)=\boldsymbol{\lambda}_b^{\mathrm{T}}\mathbf{F}. \tag{6}$$

According to the orthogonality of the main modal shape [13], Eq. (7) can be obtained from Eqs. (5) and (6).

$$\begin{cases}\boldsymbol{\lambda}_b^{\mathrm{T}}\mathbf{M}\boldsymbol{\lambda}_a\\ \boldsymbol{\lambda}_b^{\mathrm{T}}\mathbf{C}\boldsymbol{\lambda}_a\\ \boldsymbol{\lambda}_b^{\mathrm{T}}\mathbf{K}\boldsymbol{\lambda}_a\end{cases}=\begin{cases}M_a,\ a=b\\ C_a,\ a=b\\ K_a,\ a=b\\ 0,\ a\neq b\end{cases}. \tag{7}$$

Substituting Eq. (7) into Eq. (6), then,

$$M_a\ddot{q}_a+C_a\dot{q}_a+K_a q_a=\boldsymbol{\lambda}_a^{\mathrm{T}}\mathbf{F}=\boldsymbol{\lambda}_b^{\mathrm{T}}\mathbf{F}. \tag{8}$$

The excitation loading and displacement response in Eq. (8) are expressed in complex form as follows.

$$\begin{cases}\mathbf{F}=\mathbf{f}e^{j\omega t}\\ q_a=Q_a e^{j\omega t}\end{cases}. \tag{9}$$

Substituting Eq. (9) into Eq. (8),

$$Q_a=\frac{\boldsymbol{\lambda}_a^{\mathrm{T}}\mathbf{f}}{-\omega^2 M_a+j\omega C_a+K_a}. \tag{10}$$

Substituting Eqs. (10) and (9) into Eq. (4), $\mathbf{S}^{\mathrm{T}}$ can be obtained as Eq. (11).

$$\mathbf{S}^{\mathrm{T}}=\sum_{a=1}^{n}\frac{\boldsymbol{\lambda}_a^{\mathrm{T}}\mathbf{f}e^{j\omega t}\boldsymbol{\lambda}_a}{-\omega^2 M_a+j\omega C_a+K_a}. \tag{11}$$

It is assumed that the system has two points: *o* and *p*, substitute Eqs. (11) and (9) into Eq. (4), the response amplitude of the point *p* can be expressed as follows.

$$S_p=\sum_{a=1}^{n}\frac{\lambda_{oa}F_o\lambda_{pa}}{K_a\left[2j\xi_a\left(\frac{M_a\omega\sqrt{K_a/M_a}}{K_a}\right)-\frac{\omega^2 M_a}{K_a}+1\right]}. \tag{12}$$

Their frequency response function (FRF) is as Eq. (13).

$$H_{po}=\frac{S_p}{F_o}=\sum_{a=1}^{n}\frac{\lambda_{oa}\lambda_{pa}}{K_a\left[2j\xi_a\left(\frac{M_a\omega\sqrt{K_a/M_a}}{K_a}\right)-\frac{\omega^2 M_a}{K_a}+1\right]}. \tag{13}$$

According to the linear superposition assumption [12], when $\mathbf{F}=\begin{bmatrix}F_1 & F_2 & \cdots & F_N\end{bmatrix}^{\mathrm{T}}$, the response amplitude of each point of the system is as Eq. (14).

$$\mathbf{S}=\begin{bmatrix}S_1\\ S_2\\ \vdots\\ S_N\end{bmatrix}=\begin{bmatrix}H_{11} & H_{12} & \cdots & H_{1N}\\ H_{21} & H_{22} & \cdots & H_{2N}\\ \vdots & \vdots & \ddots & \vdots\\ H_{N1} & H_{N2} & \cdots & H_{NN}\end{bmatrix}\begin{bmatrix}F_1\\ F_2\\ \vdots\\ F_N\end{bmatrix}. \tag{14}$$

2.2 Parameter Identification

Since the excitation of the roof bolter includes all DOF in space, and each subsystem has $m(6)$ inputs and $n(6)$ outputs, the frequency response of each subsystem of the manipulator is a $6\times6^{\text{th}}$ order matrix, as follows.

$$\mathbf{H}_{\mathrm{J}_i}=\begin{bmatrix}H_{11}(\mathrm{J}_i) & H_{12}(\mathrm{J}_i) & \cdots & H_{16}(\mathrm{J}_i)\\ H_{21}(\mathrm{J}_i) & H_{22}(\mathrm{J}_i) & \cdots & H_{26}(\mathrm{J}_i)\\ \vdots & \vdots & \ddots & \vdots\\ H_{61}(\mathrm{J}_i) & H_{62}(\mathrm{J}_i) & \cdots & H_{66}(\mathrm{J}_i)\end{bmatrix}. \tag{15}$$

The parameters of the J_1 to J_6 frequency response curves are identified in the frequency domain [14] by the rational polynomial method [15]. Its mathematical model is a rational formula of frequency response function, as follows.

$$H_{\mathrm{mn}}(\mathrm{J}_i)=\frac{\alpha_1x^5+\alpha_2x^4+\alpha_3x^3+\alpha_4x^2+\alpha_5x+\alpha_6}{\beta_1x^5+\beta_2x^4+\beta_3x^3+\beta_4x^2+\beta_5x+\beta_6}. \tag{16}$$

3 EXTERNAL EXCITATION LOADING

3.1 Excitation from Roof Bolter

Force and moment on roof bolter: $\mathbf{F}_g$, $\mathbf{F}_a$, $\mathbf{F}_z$, $\mathbf{F}_c$, and $\mathbf{M}_d$. The direction of $\mathbf{F}_g$, $\mathbf{F}_a$ and $\mathbf{F}_z$ is along the shaft of the roof bolter, and their vector expressions is as follows.

$$\begin{cases} \mathbf{F}_g = \begin{bmatrix} F_g & 0 & 0 & 0 & 0 & 0 \end{bmatrix} \\ \mathbf{F}_z = \begin{bmatrix} F_z & 0 & 0 & 0 & 0 & 0 \end{bmatrix} \\ \mathbf{F}_a = \begin{bmatrix} F_a & 0 & 0 & 0 & 0 & 0 \end{bmatrix} \end{cases}. \quad (17)$$

The direction of $\mathbf{M}_d$ is along the shaft of the roof bolter, and its vector expression is as follows.

$$\mathbf{M}_d = \begin{bmatrix} 0 & 0 & 0 & M_d & 0 & 0 \end{bmatrix}. \quad (18)$$

While the lateral displacement of the roof bolter is greater than the distance of them, the roof bolter will collide with rock-soil. The collision force in the z and y axes is as following [16], respectively.

$$\begin{cases} F_{cz} = \begin{cases} -k\left|v(t)\right| - \Omega \operatorname{sgn} v(t) & \left|v(t)\right| \geq \Omega \\ 0 & \text{else} \end{cases} \\ F_{cy} = \begin{cases} -k\left|w(t)\right| - \Omega \operatorname{sgn} w(t) & \left|w(t)\right| \geq \Omega \\ 0 & \text{else} \end{cases} \end{cases}. \quad (19)$$

Eq. (19) is expressed in matrix form as follows.

$$\mathbf{F}_c = \begin{bmatrix} 0 & F_{cz} & F_{cy} & 0 & \frac{F_{cz}D}{2} & \frac{-F_{cy}D}{2} \end{bmatrix}. \quad (20)$$

The excitation from the roof bolter at the tip of the manipulator is as Eq. (21).

$$\mathbf{F}_\eta = \begin{bmatrix} F_a + F_g - F_z & F_{cz} & F_{cy} & M_d & \frac{F_{cz}D}{2} & \frac{-F_{cy}D}{2} \end{bmatrix}. (21)$$

3.2 Excitation to Pedestal

Force and torque on pedestal: $\mathbf{F}_{g2}$, $\boldsymbol{\tau}_1$. Each joint of the manipulator can rotate independently. To accurately describe the mechanical properties of the excitation transmitted to the pedestal through the joints of the manipulator, a force Jacobian matrix of the manipulator is introduced [17]. The transfer relationship between the excitation and the joint generalized driving force is as follows [18].

$$\boldsymbol{\tau} = \mathbf{J}(q)^{\mathrm{T}} \mathbf{F} \quad (22)$$

The torques of each joint of the manipulator is as follows (Eq. (23)).

$$\boldsymbol{\tau} = \begin{bmatrix} \tau_1 \\ \tau_2 \\ \tau_3 \\ \tau_4 \\ \tau_5 \\ \tau_6 \end{bmatrix} = \begin{bmatrix} J_{1x} & J_{2x} & -d_4(c_4c_5c_6 - s_4s_6) + a_3(s_5c_6) & 0 & 0 & 0 \\ J_{1y} & J_{2y} & d_4(c_4c_5c_6 + s_4s_6) - a_3(s_5c_6) & 0 & 0 & 0 \\ J_{1z} & J_{2z} & d_4c_4s_5 + a_3c_6 & 0 & 0 & 0 \\ -s_{23}(c_4c_5c_6 - s_4s_6) - c_{23}s_5c_6 & -s_4c_5c_6 - c_4s_6 & -s_4c_5c_6 - c_4s_6 & s_5c_6 & -s_6 & 0 \\ s_{23}(c_4c_5c_6 - s_4s_6) + c_{23}s_5c_6 & s_4c_5s_6 - c_4c_6 & s_4c_5c_6 - c_4c_6 & -s_5s_6 & -c_6 & 0 \\ s_{23}c_4s_5 - c_{23}c_5 & s_4s_5 & s_4s_5 & c_5 & 0 & 1 \end{bmatrix} \begin{bmatrix} F_x \\ F_y \\ F_z \\ M_x \\ M_y \\ M_z \end{bmatrix}, \quad (23)$$

where $J_{1x} = -d_2\left[c_{23}(c_4c_5c_6 - s_4s_6) - s_{23}s_5c_6\right] - (a_2c_2 + a_3c_{23} - d_4s_{23})(s_4c_5c_6 + c_4s_6)$; $c_i = \cos(\theta_i)$; $s_i = \sin(\theta_i)$;

$J_{1y} = -d_2\left[-c_{23}(c_4c_5c_6 + s_4s_6) + s_{23}s_5c_6\right] + (a_2c_2 + a_3c_{23} - d_4s_{23})(s_4c_5c_6 - c_4s_6)$; $s_{23} = \sin(\theta_2 + \theta_3)$;

$c_{23} = \cos(\theta_2 + \theta_3)$; $J_{1z} = d_2(c_{23}c_4s_5 + s_{23}c_5) + (a_2c_2 + a_3c_{23} - d_4s_{23})(s_4s_5)$;

$J_{2x} = a_3s_5c_6 - d_4(c_4c_5c_6 - s_4s_6) + a_2\left[s_3(c_4c_5c_6 - s_4s_6) + c_3s_5c_6\right]$;

$J_{2y} = -a_3s_5c_6 - d_4(-c_4c_5c_6 - s_4s_6) + a_2\left[s_3(-c_4c_5c_6 - s_4s_6) + c_3s_5c_6\right]$; $J_{2z} = a_3c_6 + d_4c_4s_5 + a_2(-s_3c_4s_5 + c_3c_6)$;

$F_x = F\sin\gamma\cos\varphi$; $F_y = F\sin\gamma\cos\varphi$; $F_z = F\cos\gamma$.

4 CASE IN ENGINEERING PRACTICE

4.1 Essential Parameters

A 6-DOF manipulator for anchor drilling in a coal mine in Huainan, China, is taken as the research object. The size of the two-wing drill adopted is $\phi 32$ mm; the length of drill string is 86 mm. The drilling object is sandstone, and its mechanical parameters [19] are as follows: ρ = 2600 kg/m³; R = 38 MPa; R_m = 0.34 MPa; E = 12 GPa; μ = 0.25; F_a = 6000 N; M_d =130 N; Ω = 0 mm; $k = 10^9$ N·m^{-1}; self-weight of the roof bolter is 40 kg; self-weight of the manipulator is 550 kg. Moreover, the parameters of the linkages of the manipulator are shown in Table 1 [20].

The three-dimensional model of the manipulator is shown in Fig. 2. Some finite element models of the manipulator are established, as shown in Fig. 3. The rotating joints of the manipulator are divided into some subsystems, and its exciting points and response points are determined.

Based on MTPA and MSM, the computation flow chart of the vibration transfer of 6-DOF manipulator for anchor drilling is shown Fig. 4.

Table 1. *Parameters of the linkages of the manipulator*

Linkages	Angle variable	a_{i-1} [m]	d_i [m]	Angle range [rad]
1		0	0.56	–3.14 to 3.14
2		0.90	0	–2.27 to 1.22
3		0.16	0	–1.40 to 3.05
4		0	1.01	–6.28 to 6.28
5		0	0	–2.09 to 2.09
6		0	0.2	–6.28 to 6.28

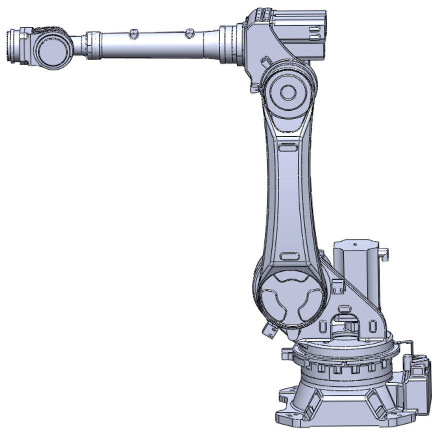

Fig. 2. *The three-dimensional model of the manipulator*

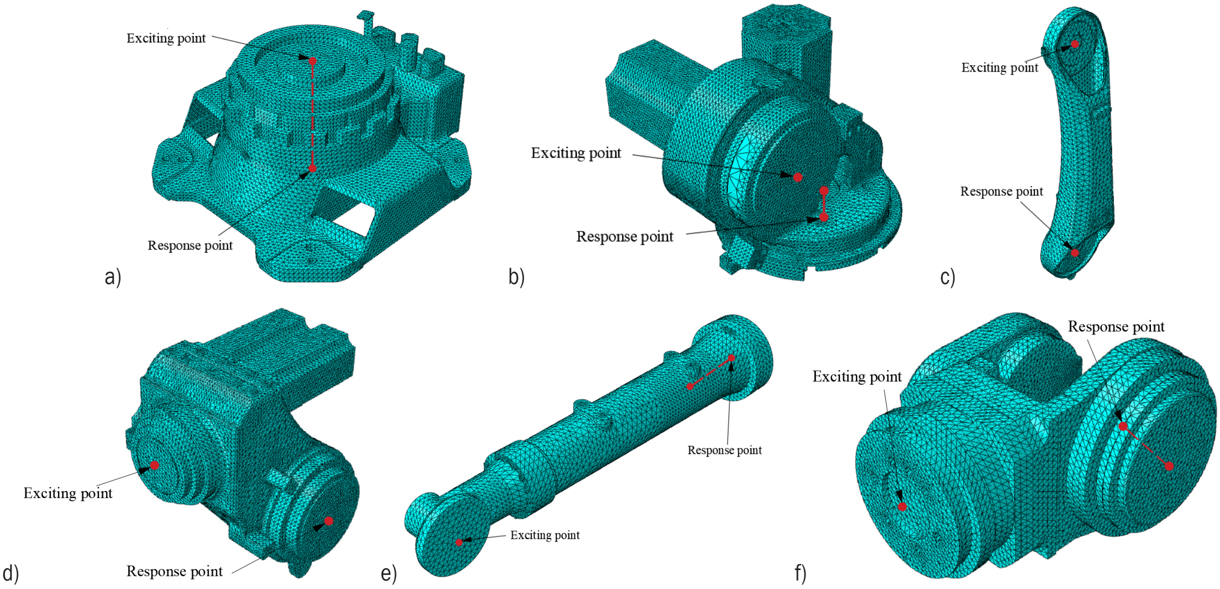

Fig. 3. *Grid division of subsystems and exciting points, response points; a)* J_1, *b)* J_2, *c)* J_3, *d)* J_4, *e)* J_5, *f)* J_6

4.2 Frequency Response Curves

The excitation of the roof bolter is high-frequency vibration; the frequency range in practice is 0 Hz to 200 Hz [21]. Substituting Eqs. (19) and (21) into Eq. (13), the frequency responses of subsystems are analysed using ABAQUS [22]. The acceleration frequency response curves of J_1 to J_6 are shown in Figs. 5 to 10.

According to Figs. 5 to 10, there are resonance peaks [23] in the frequency response curves of each subsystem of the manipulator for anchor drilling in the

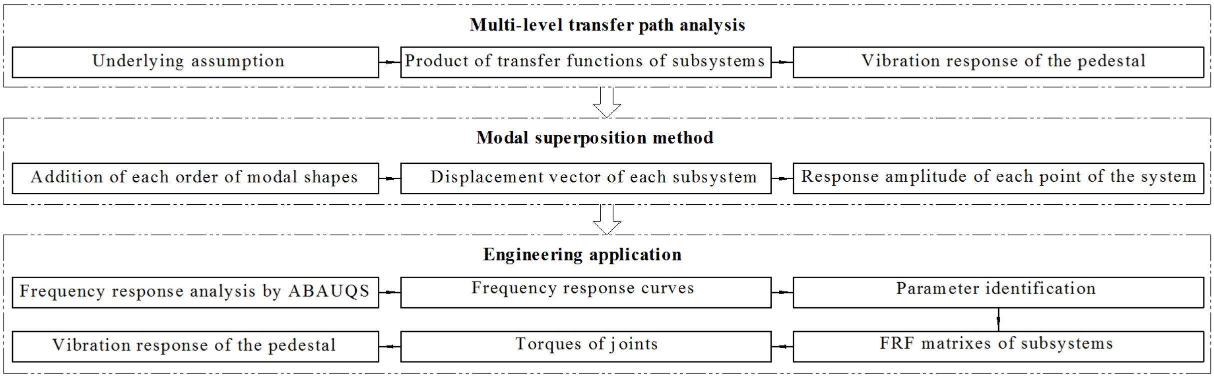

Fig. 4. *Computation flow chart*

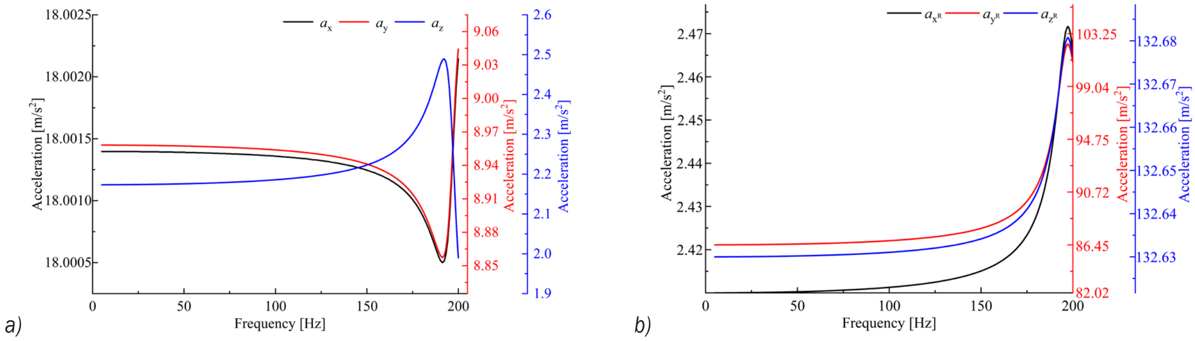

Fig. 5. *Frequency response curves of* J_1 *; a) translational acceleration, and b) rotational acceleration*

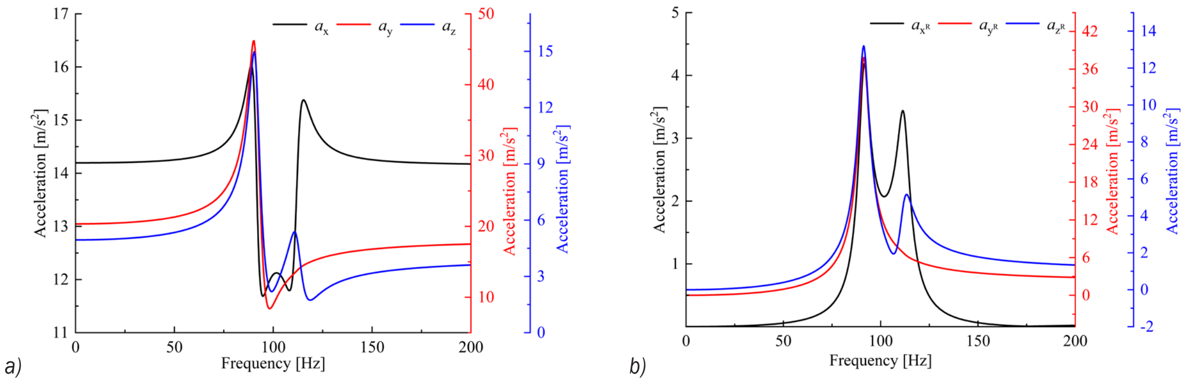

Fig. 6. *Frequency response curves of* J_2*; a) translational acceleration, and b) rotational acceleration*

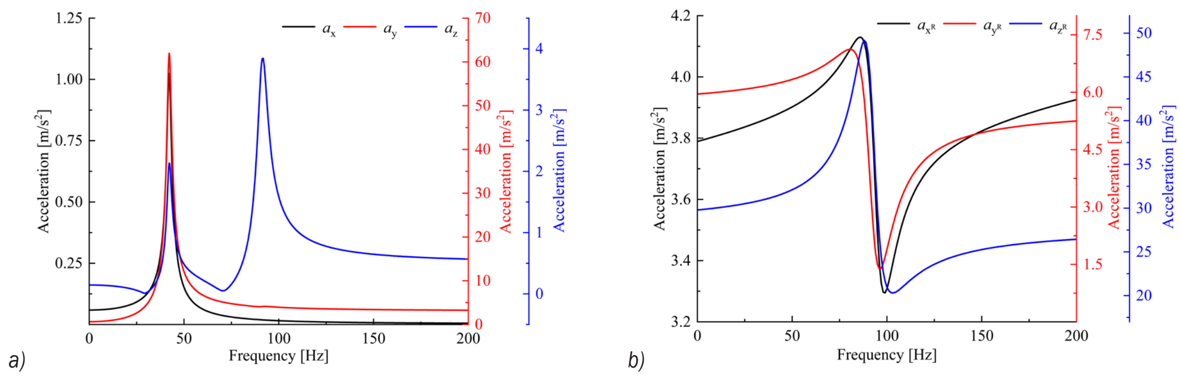

Fig. 7. *Frequency responses curve of* J_3*; a) translational acceleration, and b) rotational acceleration*

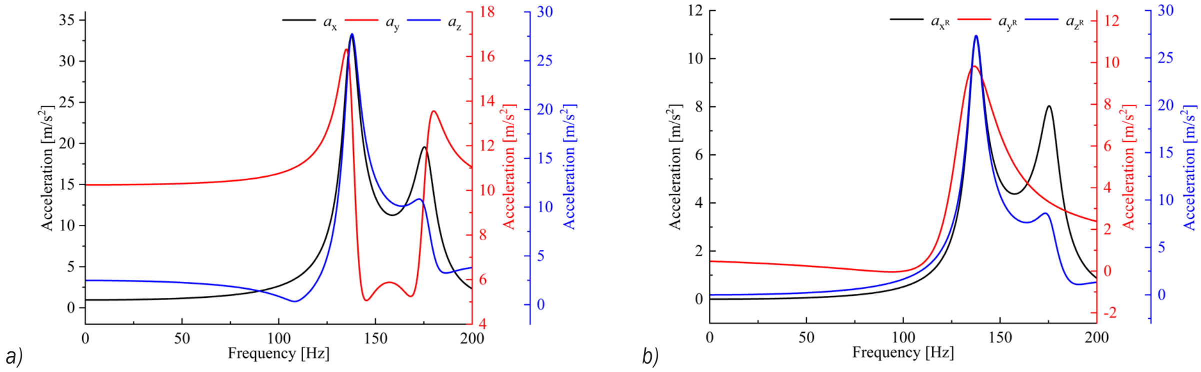

Fig. 8. *Frequency response curves of* J_4*; a) translational acceleration, and b) rotational acceleration*

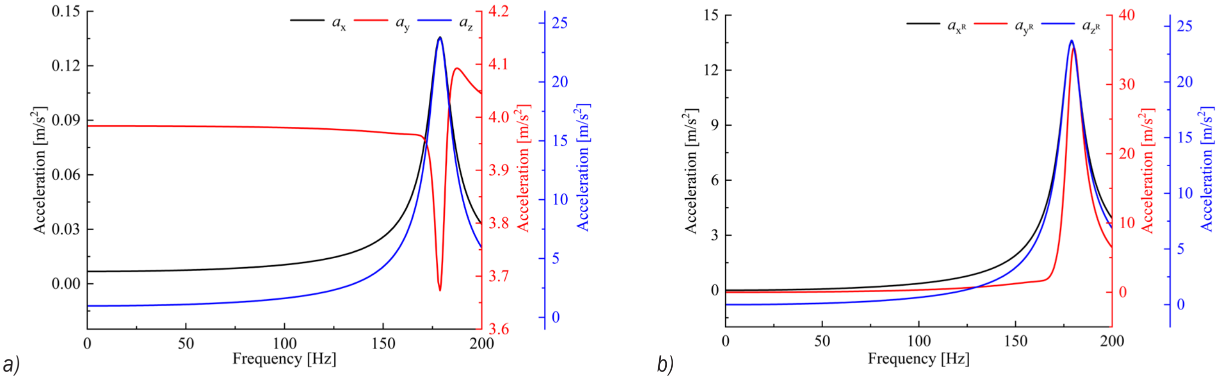

Fig. 9. *Frequency response curves of* J_5*; a) translational acceleration, and b) rotational acceleration*

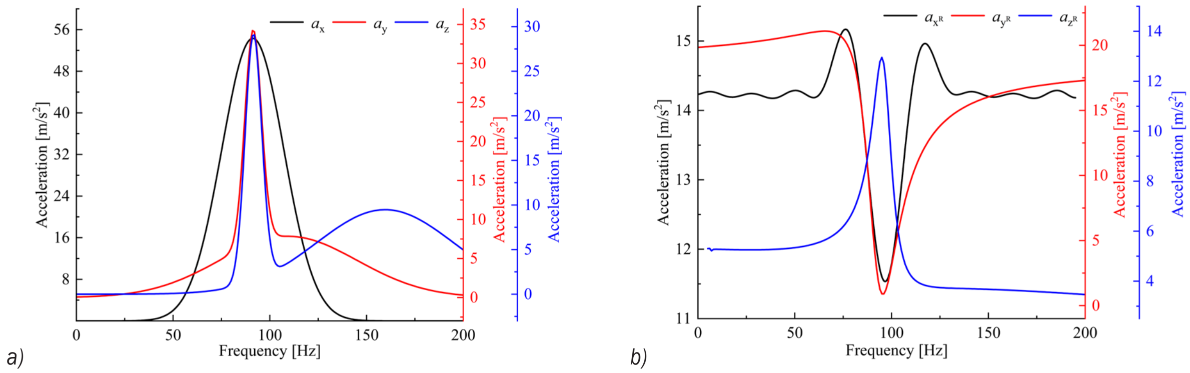

Fig. 10. *Frequency response curves of* J_6*; a) translational acceleration, and b) rotational acceleration*

frequency range of 0 Hz to 200 Hz. The frequencies corresponding to the peak values of the 6-DOF frequency response curves is shown in Table 2.

4.3 FRF Matrixes of Subsystems

The frequency response curves of each subsystem are imported into MATLAB, which are fitted according to Eq. (16) with the "Curve Fitting Tool" toolbox [24]. The coefficients of each element in the frequency response matrixes are shown in Tables 3 to 8.

Table 2. *Frequencies corresponding to peak values*

Joints	DOF Frequencies					
	x	y	z	x^R	y^R	z^R
J_1	191.3	191.3	192.2	197.3	197.4	197.2
J_2	88.95	90.32	90.32	91.55	91.34	91.24
J_3	42.19	42.19	91.77	86.2	82.9	88.1
J_4	137.5	135.2	137.9	135.3	137.8	137.8
J_5	178.8	187.4	178.8	187.4	178.7	178.8
J_6	91.27	91.34	91.54	81.66	73.24	95.54

Table 3. *Coefficients of* $H_{mn}(\mathrm{J}_1)$

Coefficients	$H_{11}(\mathrm{J}_1)$	$H_{12}(\mathrm{J}_1)$	$H_{13}(\mathrm{J}_1)$	$H_{14}(\mathrm{J}_1)$	$H_{15}(\mathrm{J}_1)$	$H_{16}(\mathrm{J}_1)$
α_1	1.053×10^{-5}	-2.359×10^{-4}	0	–0.04122	–2.474	–3.082
α_2	18	7.91×10^{-4}	5.53×10^{-4}	9.311	569.6	708.6
α_3	–14.27	8.967	-2.796×10^{-3}	–99.29	–8613	-1.05×10^{4}
α_4	–6.116	–9.886	2.15	–988.8	18.74	–328.7
α_5	3.172	–0.2581	–3.32	–155.4	58.47	7.649
α_6	1.583	2.063	1.303	–22.72	11.5	3.809
β_1	0	0	0	1	1	1
β_2	1	0	0	–398.7	–398.8	–398.8
β_3	–0.793	1	0	3.98×10^{4}	3.983×10^{4}	3.982×10^{4}
β_4	–0.3398	–1.105	1	1979	376.4	1047
β_5	0.1762	-2.802×10^{-2}	–1.519	204.9	–200.2	–50.2
β_6	0.08792	0.2307	0.5861	30.14	–35.51	–10.31

Table 4. Coefficients of $H_{mn}(\mathrm{J}_2)$

Coefficients	$H_{11}(\mathrm{J}_2)$	$H_{12}(\mathrm{J}_2)$	$H_{13}(\mathrm{J}_2)$	$H_{14}(\mathrm{J}_2)$	$H_{15}(\mathrm{J}_2)$	$H_{16}(\mathrm{J}_2)$
α_1	14.37	0	0	0	0	0
α_2	–5269	18.7	1345	0	0.01195	8.488×10^{-3}
α_3	7.419×10^{5}	–4285	-2.042×10^{5}	0	–1.265	–1.264
α_4	-4.749×10^{7}	3.445×10^{5}	2.55×10^{6}	93.75	–30.33	28.8
α_5	1.163×10^{9}	-1.361×10^{7}	4.565×10^{8}	-1.865×10^{4}	5454	1803
α_6	4.135×10^{7}	3.364×10^{8}	-4.691×10^{8}	9.654×10^{5}	-2.66×10^{4}	–9660
β_1	1	0	1	0	0	0
β_2	–367.8	1	26.8	1	0	0
β_3	5.199×10^{4}	–221.8	-1.898×10^{4}	–406	1	1
β_4	-3.341×10^{6}	1.735×10^{4}	-2.815×10^{5}	6.166×10^{4}	–185.9	–185.8
β_5	8.21×10^{7}	-6.762×10^{5}	9.554×10^{7}	-4.15×10^{6}	9099	9093
β_6	3.09×10^{6}	1.654×10^{7}	-9.949×10^{7}	1.045×10^{8}	-4.014×10^{4}	-4.077×10^{4}

Table 5. Coefficients of $H_{mn}(\mathrm{J}_3)$

Coefficients	$H_{11}(\mathrm{J}_3)$	$H_{12}(\mathrm{J}_3)$	$H_{13}(\mathrm{J}_3)$	$H_{14}(\mathrm{J}_3)$	$H_{15}(\mathrm{J}_3)$	$H_{16}(\mathrm{J}_3)$
α_1	1.396×10^{-2}	2.342	0.4121	1.18×10^{-3}	8.639×10^{-7}	0.000374
α_2	–3.895	–276.7	–83.52	3.508	5.586	27.74
α_3	416.3	1.218×10^{4}	5613	–720	–1106	–5552
α_4	-1.863×10^{4}	-2.488×10^{5}	-1.427×10^{5}	3.802×10^{4}	5.885×10^{4}	3.039×10^{5}
α_5	2.958×10^{5}	2.244×10^{6}	1.487×10^{6}	-2.085×10^{5}	-4.029×10^{5}	-2.49×10^{6}
α_6	961	-1.232×10^{6}	–10.48	2.724×10^{5}	1.164×10^{6}	5.792×10^{6}
β_1	1	1	1	0	0	0
β_2	–183.2	–155.3	–242.3	1	1	1
β_3	1.311×10^{4}	9218	2.06×10^{4}	–194.5	–191.7	–193.6
β_4	-4.286×10^{5}	-2.496×10^{5}	-7.338×10^{5}	1.006×10^{4}	9927	1.028×10^{4}
β_5	5.332×10^{6}	2.666×10^{6}	1.026×10^{7}	-5.507×10^{4}	-6.78×10^{4}	-8.394×10^{4}
β_6	1.613×10^{4}	-1.849×10^{6}	–74.75	7.189×10^{4}	1.955×10^{5}	1.951×10^{5}

4.4 Torques of Joints

Substituting the data in Table 1 into Eq. (23), the values of τ_1 change with θ_i, γ and ϕ are obtained by MATLAB, as shown in Fig. 11. τ_1 is distributed symmetrically with the change of joint angle of the manipulator. When θ_2 is at the ultimate angle of –2.27 rad and θ_4 is at that of –6.28 rad, τ_1 is only –2209 N·m as θ_1 and θ_3 change. While $\theta_3 \in$ (–1.24 ~ 1.13) rad, τ_1 shows a trend of decay, when $\theta_3 \in$ (1.13 ~

Table 6. *Coefficients of* $H_{mn}(J_4)$

Coefficients	$H_{11}(J_4)$	$H_{12}(J_4)$	$H_{13}(J_4)$	$H_{14}(J_4)$	$H_{15}(J_4)$	$H_{16}(J_4)$
α_1	0	0	0	0	0.9853	–2.179
α_2	1.452	10.87	3.019	1.283	–174.3	1054
α_3	–542.2	–3655	–729.4	15.19	6824	-1.6×10^{5}
α_4	8.655×10^{4}	3.114×10^{5}	4.697×10^{4}	-9.851×10^{4}	8.145×10^{4}	8.051×10^{6}
α_5	-7.894×10^{6}	-6.236×10^{5}	-2.925×10^{5}	1.105×10^{7}	-6.495×10^{5}	-1.18×10^{7}
α_6	3.419×10^{8}	3.929×10^{4}	3.765×10^{5}	-3.454×10^{4}	6.07×10^{5}	5.426×10^{4}
β_1	0	0	0	1	1	1
β_2	1	1	1	–624.9	–256.5	–627.4
β_3	–538.6	–341.5	–277.6	1.458×10^{5}	1.548×10^{4}	1.606×10^{5}
β_4	1.113×10^{5}	2.958×10^{4}	2.022×10^{4}	-1.506×10^{7}	1.606×10^{5}	-1.892×10^{7}
β_5	-1.044×10^{7}	-5.924×10^{4}	-1.247×10^{5}	5.81×10^{8}	-1.351×10^{6}	8.4×10^{8}
β_6	3.746×10^{8}	3828	1.529×10^{5}	-1.813×10^{6}	1.274×10^{6}	-3.868×10^{6}

Table 7. *Coefficients of* $H_{mn}(J_5)$

Coefficients	$H_{11}(J_5)$	$H_{12}(J_5)$	$H_{13}(J_5)$	$H_{14}(J_5)$	$H_{15}(J_5)$	$H_{16}(J_5)$
α_1	0	0	0	2.245	9.23×10^{-3}	0.0141
α_2	1.223×10^{-2}	4.005	12.8	–661.9	–3.182	–5.048
α_3	–4.295	–1464	–3564	3.512×10^{4}	312.4	481
α_4	388.1	1.366×10^{5}	6.619×10^{4}	2.645×10^{6}	–6312	–3513
α_5	–31.56	-4.933×10^{5}	3.108×10^{7}	-8.582×10^{6}	5.686×10^{4}	-3.849×10^{4}
α_6	46.17	3.554×10^{5}	-2.391×10^{7}	2.1×10^{6}	436	1.514×10^{5}
β_1	0	0	0	1	0	0
β_2	1	1	1	–23.44	1	1
β_3	–346.4	–366.1	696.9	-8.757×10^{4}	–364.4	–369.2
β_4	2.834×10^{4}	3.423×10^{4}	-3.441×10^{5}	1.099×10^{7}	3.424×10^{4}	3.642×10^{4}
β_5	3.039×10^{5}	-1.237×10^{5}	3.376×10^{7}	-4.608×10^{7}	-1.834×10^{5}	-4.209×10^{5}
β_6	6662	8.921×10^{4}	-2.461×10^{7}	4.1×10^{7}	-3.878×10^{4}	1.139×10^{6}

Table 8. *Coefficients of* $H_{mn}(J_6)$

Coefficients	$H_{11}(J_6)$	$H_{12}(J_6)$	$H_{13}(J_6)$	$H_{14}(J_6)$	$H_{15}(J_6)$	$H_{16}(J_6)$
α_1	2.102×10^{-3}	–3.807	0.06361	-7.357×10^{-6}	-1.485×10^{-5}	4.141
α_2	–0.1981	1476	–14.32	3.304×10^{-3}	18.62	–834.1
α_3	–153.7	-1.796×10^{5}	1087	13.72	–3857	4.244×10^{4}
α_4	2.772×10^{4}	7.604×10^{6}	-3.055×10^{4}	–2855	2.287×10^{5}	7347
α_5	-1.185×10^{6}	-5.151×10^{7}	2.653×10^{5}	1.522×10^{5}	-2.966×10^{6}	–450.4
α_6	1.48×10^{7}	4.774×10^{7}	-4.187×10^{5}	-5.962×10^{5}	8.696×10^{6}	–211.3
β_1	0	1	0	0	0	1
β_2	1	–413.3	1	0	1	–195.1
β_3	–354.4	6.999×10^{4}	–162.5	1	–200.1	9678
β_4	4.741×10^{4}	-5.504×10^{6}	4823	–202.7	1.16×10^{4}	-1.156×10^{4}
β_5	-2.837×10^{6}	1.66×10^{8}	1.585×10^{5}	1.072×10^{4}	-1.497×10^{5}	5793
β_6	6.444×10^{7}	-1.577×10^{8}	-3.222×10^{5}	-4.198×10^{4}	4.382×10^{5}	1667

2.30) rad, τ_1 shows a steady trend; and $\theta_3 \in$ (2.30 ~ 3.04) rad, τ_1 showed a slight upward trend. When θ_6 is at the ultimate angle of –6.28 rad, τ_1 is distributed symmetrically with the change of θ_5; and $\tau_{1\,\max}=6018$ N·m. As γ and φ change, τ_1 is symmetrically distributed obviously; and $\tau_{1\,\max}=9117$ N·m. The maximum of τ_1 applied to the pedestal is 9117 N·m, which is transmitted along the 6-DOF manipulator with any position and posture in space.

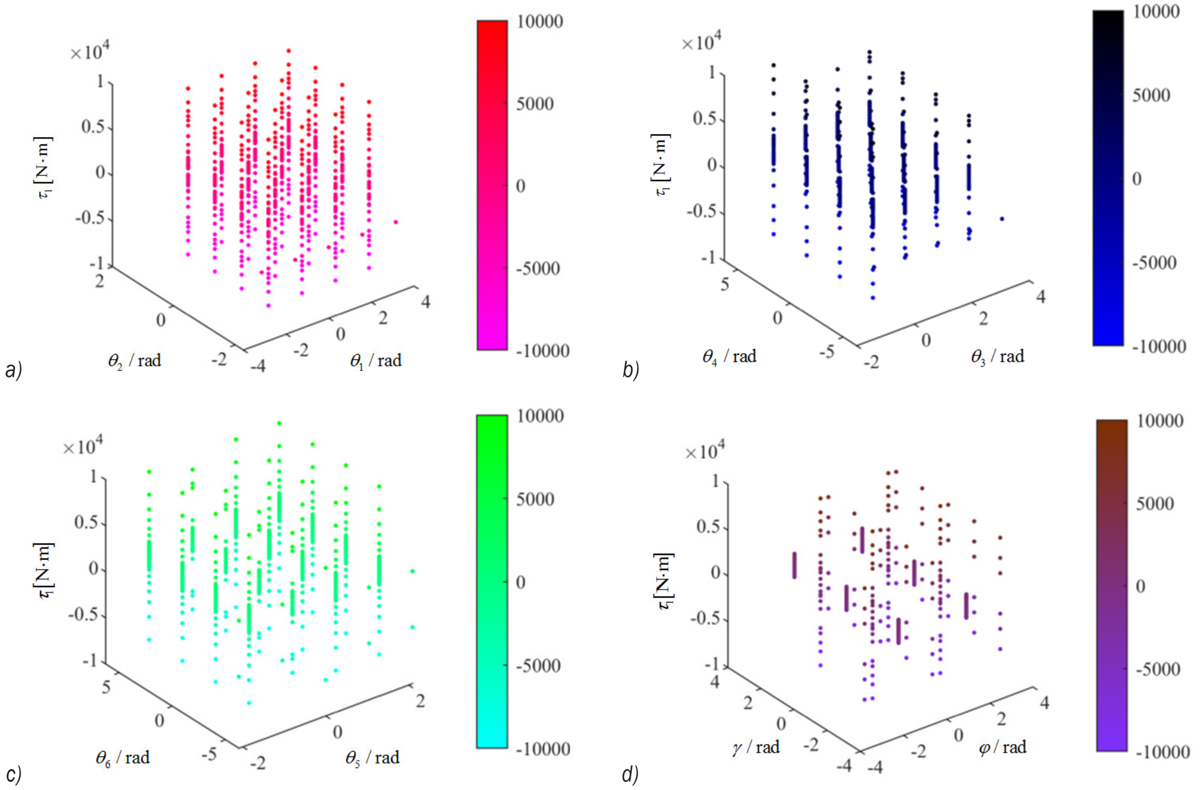

Fig. 11. τ_1 changes with θ_i (i =1 to 6), γ and φ;
a) τ_1 change with θ_1, θ_2, b) τ_1 change with θ_3 θ_4, c) τ_1 change with θ_5, θ_6, d) τ_1 change with γ, φ

4.5 Vibration Response of the Pedestal

Substituting the frequency response matrix of each subsystem into Eq. (1) and substituting Eqs. (1) and (24) into Eq. (2), the vibration responses on each DOF of the pedestal are shown in Fig. 12, in which the positive and negative values of the vibration response only represent the direction.

As shown in Fig. 12a, the response of the longitudinal vibration (S_x) of the pedestal reaches the maximum, being 1.65×10^{-2} m, when the frequency is 45 Hz. While the frequencies are 90 Hz and 180 Hz, the responses of the two components (S_y and S_z) of the bending vibration of the pedestal reach the maximum, being 2.12×10^{-2} m and 8.06×10^{-3} m, respectively. At this time, the frequencies corresponding to the peaks are integer multiples of each other, so the phenomenon of resonance will happen.

As shown in Fig. 12b, the response of the torsional vibration (S_{x^R}) of the pedestal reaches the maximum, being 9×10^{-3} m, when the frequency is 190 Hz. The two components (S_{y^R} and S_{z^R}) of rotational vibration

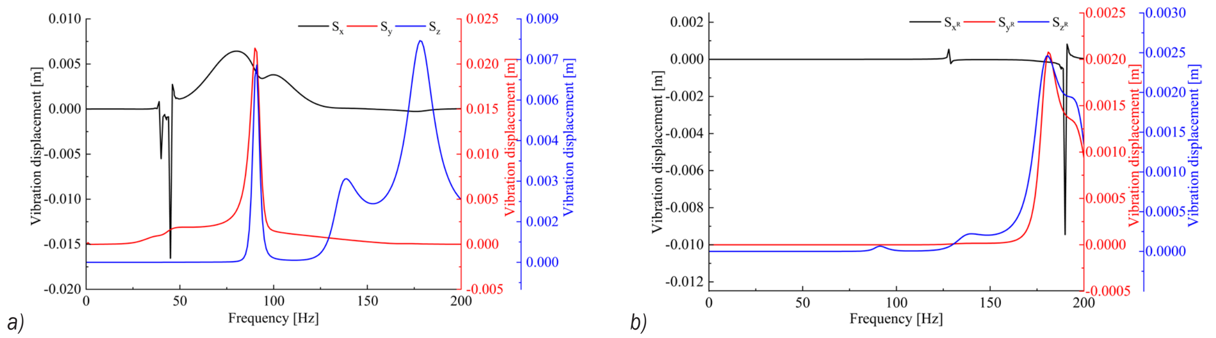

Fig. 12. Vibration responses on each DOF of the pedestal; a) vibration responses of S_x, S_y, S_z, and b) vibration responses of S_{x^R}, S_{y^R}, S_{z^R}

around y and z axes sharply increase in the frequency interval [166-181] Hz and [151-180] Hz, and reach the maximum, being 2.08×10^{-4} m and 2.46×10^{-4} m respectively, at the frequencies of 180 Hz and 181 Hz. At this time, the frequencies corresponding to the peaks are very similar, which is easy to induce a resonance. The amplitude of each DOF of the pedestal is from large to small is as follows: bending vibration (component 1) S_y, longitudinal vibration S_x, torsional vibration S_{x^R}, bending vibration (component 2) S_z, rotational vibration around z-axis S_{z^R}, rotational vibration around y-axis S_{y^R}.

5 CONCLUSIONS

(1) Based on MTPA and MSM, a mathematical model of vibration transfer of 6-DOF manipulator for anchor drilling is established. The frequency response matrix of subsystems is derived under multi-DOF excitations. When the external excitation loading is determined, the frequency response function of each DOF at the response point can be calculated by the mathematical model, which is universal for series systems.

(2) Within the frequency range (0 Hz to 200 Hz) of the excitation of the roof bolter, the corresponding frequency ranges of the peak values in the 6-DOF vibration direction of each subsystem are [191.3, 197.4] Hz, [88.95, 91.55] Hz, [42.19, 91.77] Hz, [135.2, 137.8] Hz, [178.8, 187.4] Hz and [73.24, 95.54] Hz, respectively. In the above frequency ranges, the vibration response will be the largest, and the resonance can be avoided by changing the excitation frequency of the roof bolter.

(3) A case in engineering practice shows that the amplitude of each DOF of the pedestal is from large to small is as follows: bending vibration (component 1) S_y (2.12×10^{-2} m) at 90 Hz, longitudinal vibration S_x (1.65×10^{-2} m) at 45 Hz, torsional vibration S_{x^R} (9×10^{-3} m) at 190 Hz, bending vibration (component 2) S_z (8.06×10^{-3} m) at 180 Hz, rotational vibration around z-axis S_{z^R} (2.46×10^{-4} m) at 180 Hz, rotational vibration around y-axis S_{y^R} (2.08×10^{-4} m) at 180 Hz. Obviously, the pedestal is mainly in the form of bending vibration.

(4) The case also shows that a resonance will occur among the two components of the bending vibration at the frequencies of 90 Hz and 180 Hz; a resonance among the two components of rotational vibration around the y and z axes is highly likely to occur at the frequencies of 180 Hz and 181 Hz.

The theory of vibration Transfer along the 6-DOF manipulator for anchor drilling proposed in this article can provide a theoretical foundation for the development of vibration damping techniques and the design of absorbers.

6 NOMENCLATURES

$\boldsymbol{\lambda}_a$ the a^{th} order modal shape
$\boldsymbol{\lambda}_b^T$ the b^{th} order modal shape
λ_{oa} modal shape of the o^{th} DOF of the a^{th} modal vector
λ_{pa} modal shape of the p^{th} DOF of the a^{th} modal vector
q_a modal participation factors
o exciting point
p response point
n modal order
M_a modal mass coefficient
C_a modal damping coefficient
K_a modal stiffness coefficient
$\mathbf{M}$ mass matrix
$\mathbf{C}$ damping matrix
$\mathbf{K}$ stiffness matrix
$\mathbf{S}$ vibration displacement
$\dot{\mathbf{S}}$ vibration speed
$\ddot{\mathbf{S}}$ vibration acceleration
$\mathbf{J}(q)^T$ force Jacobian matrix
J joint
J elements in Jacobian matrix
d_i distance between two adjacent linkages along the common axis [m]
a_{i-1} common perpendicular length between joint i–1 and joint i [m]
z moving DOF of z-axis
x moving DOF of x-axis
y moving DOF of y-axis
z^R rotational DOF of z-axis
x^R rotational DOF of x-axis
y^R rotational DOF of y-axis
S_y bending vibration (component 1) [m]
S_x longitudinal vibration [m]
S_z bending vibration (component 2) [m]
S_{x^R} rotational vibration around x-axis (torsional vibration) [m]
S_{y^R} rotational vibration around y-axis [m]
S_{z^R} rotational vibration around z-axis [m]
$\mathbf{F}$ external loading [N]
F_y force projected on the y-axis [N]
F_o loading at o point [N]
F_{J_i} excitation force transmitted to joints [N]
F_z force projected on the z-axis [N]
F_x force projected on the x-axis [N]

$\mathbf{F}_{g2}$ gravity of manipulator [N]
$\mathbf{F}_g$ gravity [N]
$\mathbf{F}_a$ axial thrust [N]
$\mathbf{F}_z$ disturbing force [N]
$\mathbf{F}_c$ impact force [N]
$\mathbf{M}_d$ torque
M_x torque projected on the x-axis [Nm]
M_y torque projected on the y-axis [Nm]
M_y torque projected on the z-axis [Nm]
v bending vibration displacement (component 2) [m]
w bending vibration displacement (component 1) [m]
μ Poisson's ratio
D outer diameter of drill string [m]
ρ material density [kg·m^{-3}]
R compressive strength [MPa]
R_m tensile strength [MPa]
E elastic modulus [GPa]
k elastic coefficient of impact force [N·m^{-1}]
γ angle between force and z-axis [rad]
φ angle between force and x-axis [rad]
θ_i joint angle [rad]
Ω clearance between drill string and rock-soil [mm]
ξ_a damping ratio
$\boldsymbol{\tau}$ torque matrix
$\boldsymbol{\tau}_1$ torque from the J_1-axis
α_i molecular coefficients, i = 1 to 6
β_i denominator coefficients, i = 1 to 6

7 ACKNOWLEDGEMENTS

This work was supported in part by Special Fund for Collaborative Innovation of Anhui Polytechnic University & Jiujiang District under Grant No. 2021CYXTB3, and by and by Natural Science Research Project of Higher Education of Anhui Province of China under Grant No. KJ2020A0357.

8 REFERENCES

[1] Kang, Y.S., Liu, Q.S., Xi, H.L., Gong, G.Q. (2018). Improved compound support system for coal mine tunnels in densely faulted zones: A case study of China's Huainan coal field. *Engineering Geology*, vol. 240, p. 10-20, **DOI:10.1016/j.enggeo.2018.04.006**.

[2] Liu, C.C., Zheng, X.G., Arif, A., Xu, M.B. (2020). Measurement and analysis of penetration rate and vibration on a roof bolter for identification rock interface of roadway roof. *Energy Sources, Part A: Recovery, Utilization, and Environmental Effects*, vol. 42, no. 22, p. 2751-2763, **DOI:10.1080/15567036.2019.1618987**.

[3] Shu, J.C., He E.M. (2020). Review on vibration transfer path analysis methods in frequency domain. *Mechanical Science and Technology for Aerospace Engineering*, vol. 39, no. 11, p. 1647-1655, **DOI:10.13433/j.cnki.1003-8728.20200270**.

[4] van der Seijs, M. V., de Klerk, D., Rixen, D.J. (2016). General framework for transfer path analysis: History, theory and classification of techniques. *Mechanical Systems and Signal Processing*, vol. 68-69, p. 217-244, **DOI:10.1016/j.ymssp.2015.08.004**.

[5] Lee, D.H., Lee, J.W. (2020). Operational transfer path analysis based on deep neural network: Numerical validation. *Journal of Mechanical Science and Technology*, vol. 34, p. 1023-1033, **DOI:10.1007/s12206-020-0205-5**.

[6] Yoshida, J.J., Tanaka, K.K. (2016). Contribution analysis of vibration mode utilizing operational TPA. *Mechanical Engineering Journal*, vol. 3, no. 1, p. 574-589, **DOI:10.1299/mej.15-00589**.

[7] Wang, Z.W., Zhu, P., Zhao, J.X. (2017). Response prediction techniques and case studies of a path blocking system based on global transmissibility direct transmissibility method. *Journal of Sound and Vibration*, vol. 388, p. 363-388, **DOI:10.1016/j.jsv.2016.10.020**.

[8] Guasch, O. (2009). Direct transfer functions and path blocking in a discrete mechanical system. *Journal of Sound and Vibration*, vol. 321, no. 3-5, p. 854-874, **DOI:10.1016/j.jsv.2008.10.006**.

[9] Wang, Z.W., Peng, Z.K., Liu C., Shi, X. (2019). Virtual decoupling of mechanical systems considering the mass effect of resilient links: Theoretical and numerical studies. *Mechanical Systems and Signal Processing*, vol. 123, p. 443-454, **DOI:10.1016/j.ymssp.2019.01.028**.

[10] Sakhaei, B., Durali, M. (2014). Vibration transfer path analysis and path ranking for NVH optimization of a vehicle interior. *Shock and Vibration*, vol. 2014, art. ID 697450, **DOI:10.1155/2014/697450**.

[11] Gao F., Li Y.O., Zhang J. (2015). The control strategy rseearch and engineering application of seat vibration at high speed of fr vehicle. *Proceedings of the 2015 Annual Meeting of the Chinese Society of Automotive Engineering*, p.192-195.

[12] Shah, V-.N., Bohm, G.J., Nahavandi, A.N. (1979). Modal superposition method for computationally economical nonlinear structural analysis. *Journal of Pressure Vessel Technology*, vol. 101, no. 2, p. 134-141, **DOI:10.1115/1.3454612**.

[13] Fu, Z.F., He, J.M. (2001). *Modal Analysis*. Elsevier, Woburn.

[14] Karaağaçlı T., Özgüven H.N. (2020). A frequency domain nonparametric identification method for nonlinear structures: Describing surface method. *Mechanical Systems and Signal Processing*, vol. 144, art. ID. 106872, **DOI:10.1016/j.ymssp.2020.106872**.

[15] Dong, X.G., Guo, X.Y., Wang, Y.X. (2020). Local polynomial method for frequency response function identification. *Systems Science & Control Engineering*, vol. 8, no. 1, p. 534-540, **DOI:10.1080/21642583.2020.1833784**.

[16] Piovan, M.T., Sampaio, R. (2006). Non linear model for coupled vibrations of drill-strings. *Mecanica Computacional*, p. 1751-1766.

[17] Turkovic, K., Car, M., Orsag, M.(2019). End-effector force estimation method for an unmanned aerial manipulator. *2019 Workshop on Research, Education and Development*

of Unmanned Aerial Systems, p. 96-99, **DOI:10.1109/REDUAS47371.2019.8999670**.

[18] Ding, W.H., Deng, H., Zhang, Y., Ren, Y.Q. (2012). Optimum design of the jaw clamping mechanism of forging manipulators based on force transmissibility. *Applied Mechanics and Materials*, vol. 157-158, p. 737-742, **DOI:10.4028/www.scientific.net/AMM.157-158.737**.

[19] Liu, S.W., Fu, M.X., Zhang, H. (2016). Vibration mechanism and characteristics analysis of drill rod when drilling roof bolt hole. *Journal of China University of Mining & Technology*, vol. 45, no. 5, p. 893-900, **DOI:10.13247/j.cnki.jcumt.000562**.

[20] EFORT (2019). Robot Products, from *https://www.efort.com.cn/product/prodetail/44.html*, accessed on 2019-05-09.

[21] Mendil C., Kidouche M., Doghmane M.Z., Benammar,, S., Tee, K.F. (2021). Rock-bit interaction effects on high-frequency stick-slip vibration severity in rotary drilling systems. *Multidiscipline Modeling in Materials and Structures*, vol. 17, no. 5, p. 1007-1023, **DOI:10.1108/MMMS-10-2020-0256**.

[22] Weeger O., Wever U., Simeon B. (2014). Nonlinear frequency response analysis of structural vibrations. *Computational Mechanics*, vol. 54, p. 1477-1495, **DOI:10.1007/s00466-014-1070-9**.

[23] Li, C.S., Luo, S.H., Ma, W.H. (2013). Vibration isolation performance analysis of a HXN3 diesel locomotive cab based on frequency response functions. *Journal of Vibration and Shock*, vol. 32, no. 19, p. 210-215, **DOI:10.13465/j.cnki.jvs.2013.19.025**.

[24] Grauer, J.A. (2015). An interactive MATLAB program for fitting transfer functions to frequency responses. *AIAA Scitech 2021 Forum*, p, 1-14, **DOI:10.2514/6.2021-1426**.